doi:10.1038/nature15710

Supplementary Discussion

Pulsatility in Msn2 and Mig1 dynamics

The term "pulsing" is widely used in the field of single-cell signaling dynamics to describe systems which show transitions between basal (low) and activated (high) activity states resembling those observed here[5,10,16,21,59]. In general, pulsatile dynamics can be characterized in terms of the distribution of states, the distribution of time intervals between pulsing events, and the distribution of durations of pulsing events.

Both Msn2 and Mig1 exhibit long-tailed state distributions as shown in **Extended Data Fig. 7h**. Msn2 and Mig1 exhibit monotonically decreasing pulse interval distributions (**Extended Data Fig. 7d-e**). These distributions are similar to (but not exactly) exponential (as one would expect for a memory-less Poisson-like process), with R^2>0.85 for fits to exponential functions. The deviation from a perfect exponential indicates that there are additional higher-order effects, or memory, not captured by a pure Poisson process. Both Msn2 and Mig1 exhibit unimodal pulse duration distributions as shown in **Extended Data Fig. 7f**. Mig1 has a longer tail than Msn2, indicating that some pulse events have extended durations (≥20 min), mainly at higher glucose concentrations. These extended duration events account for <10% of pulses in all cases.

To summarize, Msn2 and Mig1 both transit between basal and activated states. Their inter-pulse interval distributions are consistent with a predominantly stochastic pulse initiation process. In contrast, pulse duration distributions are unimodal with long tails, consistent with a regulated pulse termination process. These characteristics are distinct from those of oscillators (which would generate unimodal inter-pulse interval and pulse duration distributions), and distinct from those of a stochastic state-switching system (which would generate exponentials for both distributions).

Variability in single-cell data

Transcription factor nuclear localization and target gene expression are both highly variable among cells. Here, we first describe variability in the data, and then provide additional discussion about sources of variability in target gene transcription.

To show the degree of variability among cells in the single-cell data, we plot the standard deviation of nuclear localization and transcriptional responses data from the main figure (**Extended Data Fig. 1l-n**). While the cell-to-cell variability is substantial, as seen by the large standard deviations, the mean values of single-cell responses can be determined with relatively small 95% confidence intervals (see corresponding plots in the main figures). These mean single-cell responses agree well with population-based qPCR responses (**Fig. 2**).

Biological origins of variability and open challenges. In principle, we can distinguish between at least three levels of variability in this system: First, there is variability in the activities of the phosphoregulatory components that control Msn2 and Mig1 nuclear localization dynamics. Second, there is variability in the nuclear localization dynamics themselves, much of which might be driven by upstream phosphoregulatory components. Third, there is variability in the transcription of target genes. These are fluctuations that would exist even if, hypothetically, transcription factor dynamics could be made identical between cells.

The first level is currently challenging to analyze directly. However, as single-cell reporters for phosphoregulatory activities become available[61], it should increasingly be possible to better analyze phosphoregulatory fluctuations and dynamics in individual cells. The nuclear localization dynamics of Msn2 and Mig1 can be observed directly, as they are here. A major

remaining challenge is to understand how much transcription factor dynamics simply (a) follow upstream phosphoregulatory dynamics, (b) add additional processing of phosphoregulatory signals through thresholds or filters, or (c) introduce additional fluctuations, or 'noise', in the regulatory process.

At the level of target gene transcription, one source of variation is intrinsic noise in gene expression, which results from transcription occurring in stochastic bursts, and occurs even under constant conditions, without transcription factor pulsing[61,62]. This effect could add a significant layer of variability to the measured transcriptional responses (**Extended Data Fig. 1m-n** lower panels; **Extended Data Fig. 4e**). Additionally, it has been implicated previously, in analysis of the pulsatile transcription factor Crz1, that a transcription factor pulse does not necessarily lead to productive transcription, but rather increases the probability of a concomitant transcriptional burst[63]. Consistent with this picture, here we find that relative pulse timing selectively modulates the probability, and magnitude, of productive transcriptional output for the non-overlapping events, but the effects (or lack thereof) of any single pulse event on transcription are stochastic (**Extended Data Fig. 4e**). Thus, relative pulse timing modulation operates by altering the probability (or frequency) of different temporally structured events, which in turn control the probability of activation of target genes to varying extents. The existence of multiple levels of stochasticity in this system raises additional open questions: mechanistically, how do pulses control the probability of target gene activation? And functionally, does this variability impair system function (compared to a hypothetical deterministic system) or provide some type of functional advantage[64].

RNA-Seq analysis of transient responses to NaCl and ethanol

In the RNA-Seq analysis, a target was identified as an Msn2-Mig1 relative pulse timing-modulated target if it satisfied the following criteria: 1) fold-change activation in NaCl for no deletion background exceeds a predefined threshold (15%) and such change is statistically significant (with adjusted p-value from DESeq2 smaller than 0.05); 2) fold-change activation in NaCl is higher than in ethanol (larger than the threshold); 3) deletion of *mig1* leads to increased activation in ethanol compared to no deletion strain (larger than the threshold) with statistical significance. 4) fold-change activation by NaCl is still significant in *mig1* deletion background; 5) deletion of *msn2* reduced the activation by both stresses compared to no deletion strain (larger than the threshold). With these criteria, 31 targets (including *GSY1*) were identified as Msn2-Mig1 combinatorial targets (*YBR072W YBR285W YCR091W YDR516C YEL011W YER054C YER066C-A YER067C-A YFR015C YFR017C YGL037C YGR243W YHR104W YJR039W YKR058W YKR098C YLR109W YMR103C YMR104C YMR105C YMR194C-B YMR280C YMR291W YNR034W-A YOR374W YPL004C YPL230W YPR026W YPR030W YPR160W YPR184W*). Of these targets, 12 overlapped with the documented Msn2-Mig1 combinatorial targets according to Yestract.com (*YBR072W YDR516C YFR015C YGL037C YGR243W YHR104W YMR104C YMR280C YMR291W YPL004C YPR030W YPR184W*). Since the total number of documented Msn2-Mig1 targets is 328 out of all yeast ORFs, this corresponds to a p-value of 1.03×10^{-8}, validating the effectiveness of the RNA-Seq screen. It should be noted that NaCl and ethanol also induce other regulators which could presumably mask the effect we were seeking for and reduce the number of targets that passed the criteria for relative pulse timing modulation. To analyze the dependence of Msn2 and Mig1 effects on the number of the corresponding binding sites (**Extended Data Fig. 2i-k**), we scanned for possible motifs with YeTFaSCo[66] (with maximum score of 75% or higher) for each gene's promoter region (1kb

before start codon). The effect of activation by Msn2 was calculated by the averaged fold-change difference between no deletion and *msn2* deletion in response to NaCl and ethanol. Similarly, the effect of repression by Mig1 was calculated by the fold-change difference between *mig1* deletion and no deletion in response to ethanol. The results (**Extended Data Fig. 2k**) show a statistically insignificant correlation between the effect caused by either Msn2 or Mig1 and the number of corresponding motif. Thus, we were unable to conclude the effect of the number of binding motifs in endogenous targets. The strength/location of binding motif or additional binding motifs from Msn2/Mig1 or other factors could have masked the effect of motif number for these endogenous targets.

The role of delayed pulsing of Msn2 and Mig1

A distinct mode of delayed pulsing is apparent from the cross-correlation analysis (**Extended Data Fig. 7g**, i.e., peaks at time lag larger than 0) as well as the averaged overlapping Msn2/Mig1 pulses in **Fig. 3c** (i.e., second Mig1 peak). To better characterize these events, we define a delayed pulsing event as one in which an Msn2 pulse is followed by a Mig1 pulse within a 10 min window. We find that delayed pulsing events occur significantly more often than expected by chance (**Extended Data Fig. 8e**) across all glucose levels. Furthermore, we find that the relative frequency of delayed pulsing is modulated by glucose (**Extended Data Fig. 8e**). These results support the idea that delayed pulsing represents a distinct mode of relative pulse timing.

We next asked what effect delayed pulsing has on target gene expression. To do so, we further sub-divide the delayed pulsing events into non-overlapping or overlapping categories depending on whether the Msn2 and Mig1 pulses temporally overlapped. Comparing delayed overlapping events with non-delayed overlapping events, we observed relatively small and statistically insignificant difference (i.e., large overlaps of confidence intervals) in target gene expression levels (**Extended Data Fig. 4f and h**). Similarly, when we compared delayed non-overlapping pulses to non-delayed non-overlapping pulses, we also observed insignificant change in gene expression (**Extended Data Fig. 4g and i**). These results suggest that the overlapping / non-overlapping categories are more informative about gene expression, and that the additional variable of delayed or non-delayed contributes relatively little additional information about target gene expression. Nevertheless, delayed non-overlapping pulses do appear to terminate gene expression somewhat earlier than non-delayed non-overlapping pulses.

Taken together, these results suggest that delayed pulsing is indeed a distinct mode of relative pulse timing, but that it does not yet show strong effects at the level of gene expression beyond those already explained by the overlapping / non-overlapping distinction.

Analysis of gene expression data with different models

We compared the ability of three models to explain mean expression levels of Msn2-Mig1 target genes across glucose levels: (i) A model incorporating the full regulation observed, including both active and passive relative pulse timing modulation components (“active-passive”), (ii) a model that assumes independent Msn2 and Mig1 dynamics, and therefore provides only passive modulation (“passive only”); and (iii) for comparison, a hypothetical model in which Mig1 does not affect Msn2 pulses (“Msn2 only”). We note that individual target genes could have other inputs beyond Msn2 and Mig1 that influence the dependence of their expression on glucose in ways not fully accounted for by these models. Therefore we focus below primarily on the mean expression of a set of Msn2-Mig1 target genes.

Binary relative pulse timing. For simplicity, we first analyzed the data assuming only two classes of events: overlapping and non-overlapping. For each of the three models, we assumed that gene expression is proportional to the frequency of non-overlapping Msn2 pulse events, plus a basal expression level (see **Methods**). As shown in **Extended Data Fig. 8b-c**, among these three models, the active-passive model best explained the mean expression of 5 endogenous target genes (by qPCR), as well as the expression profile of each gene individually (**Extended Data Fig. 8c**). However, with the restriction of binary pulse timing we observed a systematic discrepancy between the expression predicted by the model fits and the data, specifically in the high glucose regime. The restriction to binary model evidently overestimates gene expression at high glucose.

Continuous relative pulse timing. The systematic deviation can be explained by accounting for the empirical observation that gene expression depends continuously on the time interval between Msn2 and Mig1 pulses. As shown in **Extended Data Fig. 5a-b**, gene expression exhibits a "v-shaped" dependence on the relative pulse timing of Msn2 and Mig1, with minimal expression when Mig1 temporally overlaps the Msn2 pulse, and progressively increasing expression when the relative timing between Msn2 and Mig1 increases in either direction. At higher glucose concentrations, there is a higher overall Mig1 duty cycle, so the mean interval between Msn2 and Mig1 pulses is smaller compared to lower glucose concenrtations. This can be seen in the cross-correlation functions (**Extended Data Fig. 7g**). In the continuous pulse timing analysis, each Msn2 pulse depends on its relative timing with Mig1, following the empirical dependence in **Extended Data Fig. 5b** (see **Methods** for more details). Accounting for this effect improves the agreement of the active-passive model with mean gene expression data (compare **Fig. 3i** and **Extended Data Fig. 8b**). Furthermore, the active-passive model fits the data better than the passive only or Msn2 only models. Looking at genes individually, we found that the active-passive model fits best for 4 out of the 5 genes analyzed by qPCR (**Extended Data Fig. 8c**).

Confirmation with independent RNA-seq data set. To further validate this analysis, we subsequently analyzed an independent RNA-seq gene expression data set for the same 9 glucose concentrations. We analyzed average expression from the same 28 combinatorially regulated genes identified in **Extended Data Fig. 2.** The results are plotted in **Extended Data Fig. 8d.** As with the qPCR data, the RNAseq target gene expression profiles fit best to the active-passive model, with continuous model fitting better than binary model.

Taken together, these results suggest that the active-passive model, including continuous pulse timing provides the best explanation of combinatorial target gene expression profiles. It should be noted that the responsiveness of promoter (i.e., kinetic parameters) can impact the model predicability. In the regime of very slow responding promoters, the response to pulses would be averaged out and the model would fail to explain gene expression.

The roles of stress identity and level in the modulation of relative pulse timing

In the main text, we have demonstrated that 1) stress identity modulates relative pulse timing during the transient stress response and 2) stress level modulates relative pulse timing during the steady-state responses. We performed additional experiments suggesting two additional points: 3) stress level does not appear to modulate relative pulse timing during the transient stress in a way that would reverse the type of relative timing (**Extended Data Fig. 9a**) and 4) stress identity could modulate relative pulse timing during the steady-state responses by changing the ratio between measured overlap fraction and expected overlap fraction (**Extended**

Data Fig. 9b-c). This latter modulation is also evident from the changes in cross-correlation functions (**Extended Data Fig. 9d**). Points 1-2 are reflected in the cartoon of **Fig. 4a**.

Connection between transient and steady-state responses to stresses

NaCl and ethanol caused *opposite* relative timing during transient responses (NaCl generates non-overlapping, while ethanol generates an overlapping response), but both increase the non-overlap fraction in steady-state (**Extended Data Fig. 9b-d**). This provokes the question of why the same stress (ethanol) would produce opposite relative timing effects in transient and steady-state conditions. We speculate that this behavior would allows the cell to filter out brief exposures to ethanol (not generate a transcriptional response), while still responding to prolonged exposure to the stress. As the duration of exposure increases, both stresses induce transcriptional responses, which are enhanced by increasing the fraction of non-overlapping pulsing.

The role of Glc7 in active relative pulse timing modulation

Both cross-correlation analysis (**Extended Data Fig. 7g**) and the overlap fraction analysis (**Fig. 3g** and **Extended Data Fig. 8a**) reveal a regime of active relative pulse timing modulation for Msn2 and Mig1 dynamics where the overlap fraction deviates significantly and systematically from that expected if Msn2 and Mig1 dynamics were independent. To gain mechanistic insight into this behavior, we searched for molecular components such as kinases and phosphatases that could mediate active modulation.

Previous literature has suggested that Glc7, the catalytic subunit of PP1 phosphatase, can play indirect roles in the regulation of both Msn2 and Mig1 nuclear localization in response to glucose limitation[43,66-68], suggesting that it could mediate overlapping pulsing. To test this hypothesis, we replaced the endogenous *GLC7* promoter with a copper inducible promoter in the endogenous locus, and analyzed Mig1 and Msn2 dynamics in the resulting strain using single-cell movies (**Fig. 4b** and **Extended Data Fig. 10**). When *GLC7* expression was reduced relative to its wild-type expression level (no additional copper added to media), the deviation of overlap fraction from the expectation under independence was abolished (**Fig. 4b**). More specifically, at ~50% reduced *GLC7* expression, the fraction of measured overlapping pulses became similar to that expected under the assumption that Msn2 and Mig1 dynamics are independent. Moreover, restoring the expression of *GLC7* by copper induction restored the normal (non-independent) relative pulse timing. That is, it produced a similar elevated overlapping fraction at high glucose as that observed in the wild-type strain without *GLC7* perturbation. Finally, at low glucose levels, where no active modulation was detected, *GLC7* reduction and restoration preserved the expected behavior under the assumption of independent Msn2 and Mig1 dynamics. Together, these results indicate that *GLC7* plays a role in relative pulse timing modulation, and does so specifically in the regime in which active modulation is observed under these conditions (**Fig. 4b** left panel).

In addition to analyzing the overlap fraction, we also plotted the mean cross-correlation functions from three conditions (wild-type, inducible *GLC7* mutant without induction, inducible *GLC7* mutant with induction). The cross-correlation functions showed the expected changes in relative pulse timing, in particular a reduction in the amplitude of the overlapping peak at time lag 0 for the reduced *GLC7* condition, and the restoration of this peak when *GLC7* expression was induced in the mutant (**Fig. 4b** right panel). We also plotted the distributions of pulse interval between Msn2 and its nearest Mig1 pulse for the aforementioned conditions (**Extended**

Data Fig. 10d). These distributions show that normal *GLC7* expression is necessary for the overlapping peak, around a pulse interval of 0. For completeness, we also asked if *GLC7* also plays a role in the transient overlapping pulse observed in response to ethanol stress (**Fig. 2c**). In this condition, we found that the overlapping transient response still occurred regardless of *GLC7* expression reduction (**Extended Data Fig. 10e**), indicating that other components are likely involved in relative pulse timing modulation under these different conditions.

We note that overexpression of *GLC7* beyond wild-type levels can introduce toxicity for the cell[69,70]. This prevents exploration of the effects of higher levels of *GLC7* expression. Taken together, these experiments show that the expression level of *GLC7* is critical for active modulation under low glucose steady-state conditions. However, the function of Glc7 could be regulated at the protein level, possibly through its specific interaction partners[68], rather than through changes in expression.

Supplementary Note

Relative pulse timing modulation allows the cell to tune the effective cooperativity between transcription factors

Consider the DNA binding of two transcription factors (TFs; *A* and *B*). A promoter with one binding site for each factor can exhibit one of four distinct configurations (**Table SN1**) depending on whether no factor, one factor, or both factors are bound. We can write down the statistical weight and the corresponding thermodynamic description for each of the four configurations assuming that the system obeys Boltzmann statistics[71,72] (**Table SN1**).

Configuration	Statistical Weight	Normalized statistical weight	Thermodynamic description
	$\frac{N_{ns}!}{A!\,B!\,(N_{ns}-A-B)!}e^{-(A\cdot\varepsilon_{A,ns}+B\cdot\varepsilon_{B,ns})/kT}$	1	1
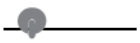	$\frac{N_{ns}!}{(A-1)!\,B!\,(N_{ns}-A-B+1)!}e^{-((A-1)\cdot\varepsilon_{A,ns}+B\cdot\varepsilon_{B,ns}+\varepsilon_{A,s})/kT}$	$\frac{A}{N_{ns}}e^{-\Delta\varepsilon_A/kT}$	$\frac{[A]}{K_A}$
	$\frac{N_{ns}!}{A!\,(B-1)!\,(N_{ns}-A-B+1)!}e^{-(A\cdot\varepsilon_{A,ns}+(B-1)\cdot\varepsilon_{B,ns}+\varepsilon_{B,s})/kT}$	$\frac{B}{N_{ns}}e^{-\Delta\varepsilon_B/kT}$	$\frac{[B]}{K_B}$
	$\frac{N_{ns}!}{(A-1)!\,(B-1)!\,(N_{ns}-A-B+2)!}e^{-((A-1)\cdot\varepsilon_{A,ns}+(B-1)\cdot\varepsilon_{B,ns}+\varepsilon_{A,s}+\varepsilon_{B,s}+\varepsilon_{AB})/kT}$	$\frac{A}{N_{ns}}\frac{B}{N_{ns}}e^{-(\Delta\varepsilon_A+\Delta\varepsilon_B+\varepsilon_{AB})/kT}$	$\omega_{AB}\frac{[A]}{K_A}\frac{[B]}{K_B}$

Table SN1 | Thermodynamic descriptions for DNA binding of two TFs. In the statistical mechanics description, N_{ns} represents the total number of non-specific binding sites, *A* and *B* represent the number of TF, $\varepsilon_{A,ns}$,$\varepsilon_{B,ns}$ and $\varepsilon_{A,s}$, $\varepsilon_{B,s}$ represent the non-specific and specific binding energies of A and B, and ε_{AB} represents the interaction energy between A and B. In the thermodynamic description, $[A]$ and $[B]$ represent the concentrations, K_A and K_B represent the dissociation constants, and $\omega_{AB} = exp(-\varepsilon_{AB}/kT)$ represents the interaction between A and B.

For concentration-modulated (CM) TFs (**Extended Data Fig. 10f**), the cooperativity ω_{AB} enhances the probability of simultaneous binding of both TFs. In this scenario, the probability of both *A* and *B* being bound can be represented as a function of cooperativity:

$$P_{AB}^{CM}(\omega_{AB}) = \frac{\omega_{AB}\frac{[A]_{CM}[B]_{CM}}{K_A K_B}}{1+\frac{[A]_{CM}}{K_A}+\frac{[B]_{CM}}{K_B}+\omega_{AB}\frac{[A]_{CM}[B]_{CM}}{K_A K_B}} \quad (1)$$

To compare with a relative pulse timing modulation system, we consider the general case of time-modulated (TM) TFs, which use frequency and/or duration modulation to control the fraction of time they are fully active (**Extended Data Fig. 10f**). In this case, we can consider four distinct states of transcription factor activation, depending on which factor or factors is active (e.g. nuclear localized) at any given moment. θ_A and θ_B denote the fraction of time that A and B, respectively, are active. Assuming A and B dynamics are independent, the fraction of time that both are activated simultaneously is $\theta_A \cdot \theta_B$, which we denote θ_{AB}. The fraction of time that only A or only B is activated is $\theta_A - \theta_{AB}$ or $\theta_B - \theta_{AB}$, respectively. Finally, the fraction of time that neither A nor B is activated is $1 - \theta_A - \theta_B + \theta_{AB}$. Therefore, we can represent the probability of both *A* and *B* being bound simultaneously to the promoter, denoted $P_{AB}^{TM}(\theta_{AB})$, as a function of the fraction of time that both are simultaneously active, θ_{AB}:

$$P_{AB}^{TM}(\theta_{AB}) = \theta_{AB}\frac{\omega_{AB}\frac{[A]_{TM}[B]_{TM}}{K_A K_B}}{1+\frac{[A]_{TM}}{K_A}+\frac{[B]_{TM}}{K_B}+\omega_{AB}\frac{[A]_{TM}[B]_{TM}}{K_A K_B}} \quad (2)$$

One can compare the effect of modulating the cooperativity or relative timing for CM and TM regulation, respectively, at the same mean regulator concentrations, i.e., $[A]_{TM} = \frac{[A]_{CM}}{\theta_A}$ and $[B]_{TM} = \frac{[B]_{CM}}{\theta_B}$ (**Extended Data Fig. 10g**). As we noted above, when the dynamics of two factors are independent, we have $\theta_{AB} = \theta_A \cdot \theta_B$. In the scenario of relative pulse timing modulation, θ_{AB} could be modulated passively by changing either or both θ_A and θ_B, or it could be modulated actively to deviate from $\theta_A \cdot \theta_B$.

Comparing Equations (1) and (2), we see that increasing either the A-B interaction energy ω_{AB} and/or the overlap fraction,θ_{AB}, increases the probability of simultaneous binding. In this sense, the ability to modulate overlap fraction allows the cell to bias the probability of simultaneous binding of two transcription factors, beyond the level expected if they are independently regulated. **Extended Data Fig. 10g** plots the probability of simultaneous binding as a function of the mean A and B concentrations (in CM) and time fractions (in TM). Thus, increasing cooperativity in CM or increasing overlapping pulsing in TM can both increase the sharpness of the response (**Extended Data Fig. 10g-h**). It should be noted that the downstream effect of overlapping pulses on gene expression may depend on the promoter kinetic parameters.

Supplementary References

59 Batchelor, E., Mock, C. S., Bhan, I., Loewer, A. & Lahav, G. Recurrent initiation: A mechanism for triggering p53 pulses in response to DNA damage. *Molecular Cell* **30**, 277-289 (2008).

60 Regot, S., Hughey, J. J., Bajar, B. T., Carrasco, S. & Covert, M. W. High-sensitivity measurements of multiple kinase activities in live single cells. *Cell* **157**, 1724-1734, (2014).

61 Golding, I., Paulsson, J., Zawilski, S. M. & Cox, E. C. Real-time kinetics of gene activity in individual bacteria. *Cell* **123**, 1025-1036 (2005).

62 Chubb, J. R., Trcek, T., Shenoy, S. M. & Singer, R. H. Transcriptional pulsing of a developmental gene. *Current Biology* **16**, 1018-1025 (2006).

63 Lubeck, E. & Cai, L. Single-cell systems biology by super-resolution imaging and combinatorial labeling. *Nature Methods* **9**, 743-U159 (2012).

64 Eldar, A. & Elowitz, M. B. Functional roles for noise in genetic circuits. *Nature* **467**, 167-173 (2010).

65 de Boer, C. G. & Hughes, T. R. YeTFaSCo: a database of evaluated yeast transcription factor sequence specificities. *Nucleic Acids Research* **40**, D169-D179 (2012).

66 Sanz, P., Alms, G. R., Haystead, T. A. J. & Carlson, M. Regulatory interactions between the Reg1-Glc7 protein phosphatase and the Snf1 protein kinase. *Molecular and Cellular Biology* **20**, 1321-1328 (2000).

67 Rubenstein, E. M. *et al.* Access denied: Snf1 activation loop phosphorylation is controlled by availability of the phosphorylated threonine 210 to the PP1 phosphatase. *The Journal of Biological Chemistry* **283**, 222-230 (2008).

68 Tabba, S., Mangat, S., McCartney, R. & Schmidt, M. C. PP1 phosphatase-binding motif in Reg1 protein of Saccharomyces cerevisiae is required for interaction with both the PP1 phosphatase Glc7 and the Snf1 protein kinase. *Cell Signal* **22**, 1013-1021 (2010).

69 Liu, H., Krizek, J. & Bretscher, A. Construction of a GAL1-regulated yeast cDNA expression library and its application to the identification of genes whose overexpression causes lethality in yeast. *Genetics* **132**, 665-673 (1992).

70 Ghosh, A. & Cannon, J. F. Analysis of protein phosphatase-1 and aurora protein kinase suppressors reveals new aspects of regulatory protein function in Saccharomyces cerevisiae. *PLoS ONE* **8**, e69133 (2013).

71 Ackers, G. K., Johnson, A. D. & Shea, M. A. Quantitative model for gene-regulation by lambda-phage repressor. *P Natl Acad Sci USA* **79**, 1129-1133 (1982).

72 Bintu, L. *et al.* Transcriptional regulation by the numbers: models. *Curr Opin Genet Dev* **15**, 116-124 (2005).

Supplementary Table 1 | Yeast strains constructed and used in this study.

#	Strain designation	Strain genotype	Used in figure
60	*MSN2-mKO2 MIG1-mCherry*	*BY4741 MSN2-mKO2::LEU2 MIG1-mCherry::spHIS5 SUC2-24xPP7::KANMX + pDZ276 (PP7-2xGFP::URA3)*	EDF 1j-k; EDF 8f-g
388	*MSN2 MIG1*	*BY4741 mig2:: HPHMX msn4::URA3 nrg1:: KANMX nrg2:: LEU2*	EDF 2f, EDF 8d
389	*MSN2 mig1*	*BY4741 mig1::spHIS5 mig2:: HPHMX msn4::URA3 nrg1:: KANMX nrg2:: LEU2*	EDF 2g
390	*msn2 MIG1*	*BY4741 msn2::spHIS5 mig2:: HPHMX msn4::URA3 nrg1:: KANMX nrg2:: LEU2*	EDF 2h, 8d
404	*MSN2-mKO2 MIG1-mCherry GSY1-24xPP7SL PP7-2xGFP*	*BY4741 MSN2-mKO2::LEU2 MIG1-mCherry::spHIS5 GSY1-24xPP7::KANMX msn4Δ mig2Δ nrg1::HPHMX nrg2::Met15 SUC2::NatMX + pDZ276 (PP7-2xGFP::URA3)*	1b; 3a-g; 4b; EDF 1g-i,l; EDF 2c-e; EDF 3b; EDF 4d-i; EDF 5b-c; EDF 6; EDF 7; EDF 8a, e; EDF 9
412	*MSN2-mKO2 MIG1(ZFΔ)-mCherry GSY1-24xPP7SL PP7-2xGFP*	*BY4741 MSN2-mKO2::LEU2 MIG1(Δaa36-91)-mCherry::spHIS5 GSY1-24xPP7::KANMX msn4Δ mig2Δ nrg1::HPHMX nrg2::Met15 SUC2::NATMX + pDZ276 (PP7-2xGFP::URA3)*	EDF 4a-b, d; EDF 5e
439	*MSN2(ZFΔ)-mKO2 MIG1-mCherry GSY1-24xPP7SL PP7-2xGFP*	*BY4741 MSN2(Δaa642-704)-mKO2::LEU2 MIG1-mCherry::spHIS5 GSY1-24xPP7::KANMX msn4Δ mig2Δ nrg1::HPHMX nrg2::Met15 SUC2::NATMX + pDZ276 (PP7-2xGFP::URA3)*	EDF 4a-b, d; EDF 5e

441	*MSN2-mKO2 MIG1-mCherry (STRE)$_4$(Mig1)$_2$-24xPP7SL PP7-2xGFP*	*BY4741 MSN2-mKO2::LEU2 MIG1-mCherry::spHIS5 trp1::(STRE)$_4$(Mig1)$_2$-PHIS3-24xPP7::KANMX msn4Δ mig2Δ nrg1::HPHMX nrg2::Met15 SUC2::NATMX + pDZ276 (PP7-2xGFP::URA3)*	2b-e; 3d-e; EDF 1a,d,g, m-n; EDF 3a; EDF 4c, e-i; EDF 5a
442	*MSN2-mKO2 MIG1-mCherry (STRE)$_4$-24xPP7SL PP7-2xGFP*	*BY4741 MSN2-mKO2::LEU2 MIG1-mCherry::spHIS5 trp1::(STRE)$_4$-PHIS3-24xPP7::KANMX msn4Δ mig2Δ nrg1::HPHMX nrg2::Met15 SUC2::NATMX + pDZ276 (PP7-2xGFP::URA3)*	2d-e; EDF 1b, e; EDF 4a-c; EDF 5d
443	*MSN2-mKO2 MIG1-mCherry (Mig1)$_2$-24xPP7SL PP7-2xGFP*	*BY4741 MSN2-mKO2::LEU2 MIG1-mCherry::spHIS5 trp1::(Mig1)$_2$-PHIS3-24xPP7::KANMX msn4Δ mig2Δ nrg1::HPHMX nrg2::Met15 SUC2::NATMX + pDZ276 (PP7-2xGFP::URA3)*	2d-e; 3f; EDF 1c,f; EDF 4a-c; EDF 5d
447	*MSN2 MIG1 (STRE)$_4$(Mig1)$_2$-mKO2*	*BY4741 mig2::HPHMX msn4::URA3 nrg1::KANMX nrg2::LEU2 trp1:: (STRE)$_4$(Mig1)$_2$-PHIS3-mKO2::NATMX*	2f; EDF 2a-b; EDF 8b-c
448	*MSN2 MIG1 (STRE)$_4$-mKO2*	*BY4741 mig2::HPHMX msn4::URA3 nrg1::KANMX nrg2::LEU2 trp1:: (STRE)$_4$-PHIS3-mKO2::NATMX*	2f
449	*MSN2 MIG1 (Mig1)$_2$-mKO2*	*BY4741 mig2::HPHMX msn4::URA3 nrg1::KANMX nrg2::LEU2 trp1:: (Mig1)$_2$-PHIS3 -mKO2::NATMX*	2f
450	*msn2 MIG1 (STRE)$_4$(Mig1)$_2$-mKO2*	*BY4741 msn2::spHIS5 mig2::HPHMX msn4::URA3 nrg1::KANMX nrg2::LEU2 trp1:: (STRE)$_4$(Mig1)$_2$-PHIS3 -mKO2::NATMX*	EDF 2a-b
451	*MSN2-mKO2 MIG1-mCherry GSY1-24xPP7SL*	*BY4741 MSN2-mKO2::LEU2 MIG1-mCherry::spHIS5 GSY1-24xPP7::KANMX msn4Δ mig2Δ nrg1::HPHMX nrg2::Met15 SUC2::NatMX*	EDF 10b
452	*MSN2 mig1 (STRE)$_4$(Mig1)$_2$-mKO2*	*BY4741 mig1::spHIS5 mig2::HPHMX msn4::URA3 nrg1::KANMX nrg2::LEU2 trp1:: (STRE)$_4$(Mig1)$_2$-PHIS3 -mKO2::NATMX*	EDF 2a-b

453	*MSN2-mKO2 MIG1-mCherry CUP1-GLC7 GSY1-24xPP7SL*	*BY4741 MSN2-mKO2::LEU2 MIG1-mCherry::spHIS5 GSY1-24xPP7::KANMX msn4Δ mig2Δ nrg1::HPHMX nrg2::Met15 SUC2::NatMX GLC7p::URA3-PCUP1-GLC7*	4b; EDF 10